Materials Science in Semiconductor Processing 42 (2016) 215–218

Contents lists available at ScienceDirect

Materials Science in Semiconductor Processing

journal homepage: www.elsevier.com/locate/mssp

Te implantation in Ge(001) for *n*-type doping applications

J. Perrin Toinin [a,*], A. Portavoce [b], K. Hoummada [a], M. Texier [a], M. Bertoglio [b], S. Bernardini [a], L. Chow [c]

[a] Aix-Marseille University, IM2NP, Faculté des Sciences de Saint-Jérôme case 142, 13397 Marseille, France
[b] CNRS, IM2NP, Faculté des Sciences de Saint-Jérôme case 142, 13397 Marseille, France
[c] Department of Physics, University of Central Florida, Orlando, FL 32816, USA

ARTICLE INFO

Article history:
Received 27 May 2015
Received in revised form
17 July 2015
Accepted 27 July 2015
Available online 3 August 2015

Keywords:
Germanium
Tellurium
n-Type doping
Implantation
Dislocations
Clusters

ABSTRACT

5×10^{15} Te^+ ions cm^{-2} were implanted in an Ge(001) substrate using an industrial implanter with a Te^+ beam energy of 180 keV. In addition to usual implantation-mediated defects observed in Ge with usual dopants, Te implantations lead to the formation of amorphous surface GeO clusters exhibiting micrometer scale sizes, as well as deep extended defects. Implantation defects promote the formation of two distributions of dislocation loops and clusters located at two different depths in the Ge substrate during annealing. No interactions between Te atoms and dislocation loops were observed. However, the formation of non-equilibrium Te–Ge clusters, probably mediated by Ge self-interstitials, was found to prevent the Te solubility to exceed $\sim 5 \times 10^{19}$ cm^{-3} in Ge. The regular implantation method is shown to be ineffective for the production of high level *n*-type Ge doping using Te, due to the important Ge damage caused by Te implantation.

1. Introduction

Due to physical limitations that can be reached soon with the Si complementary metal–oxide–semiconductor (CMOS) technology due to ongoing successful device size reductions, efforts are currently put into technical solutions allowing for the shift from the Si technology to the closest semiconductor technology based on the use of Ge. Indeed, Ge has been already introduced in the Si CMOS technology and presents several benefits compared to Si, such as faster charge carrier mobility, smaller band gap, and lower process thermal budget [1] However, despite interesting results concerning defect-free Ge substrate production [2,3], high-k dielectric fabrication [4], and electrical contact fabrication [5], the Ge CMOS technology development difficulties are mainly linked to the difficulty of high level *n*-type Ge doping production. Indeed, despite that reliable and efficient Ge-based devices have been demonstrated [6], the sizes of these devices cannot be reduced to similar sizes as Si-based devices due to the stronger diffusivity and the lower solubility limit of usual dopants in Ge. Te doping in Ge has been poorly studied until now. However, Te atoms being double donors in Ge, Te doping could be a reliable solution for *n*-type Ge doping.

In this work, the usual doping process based on atomic implantation followed by thermal annealing is investigated in the case of Te doping in Ge. A significant dose of Te atoms, allowing for a bulk concentration of 5×10^{20} Te atoms cm^{-3} was implanted in an Ge(001) substrate using an industrial implanter. The defects created in the Ge substrate and their interactions with Te atoms were studied by electron microscopy and atom probe tomography after implantation and post-implantation annealing. High dose Te implantation is shown to lead to significant implantation-mediated defects promoting the formation of dislocation loops and Te–Ge clusters during post-implantation annealing that are not compatible with an efficient Ge CMOS technology.

2. Experiments

A dose of 5×10^{15} Te^+ ions cm^{-2} was implanted into a four inch Ga-doped Ge(001) substrate exhibiting a bulk resistivity of 0.059–0.088 Ω cm, using the industrial implanter IMC200 developed by the company IBS with a Te^+ ion energy of ~180 keV. After implantation, the Ge substrate was cut into several pieces of 1×1 cm^2 and part of the samples were simultaneously annealed at 650 °C for 1 h under vacuum ($P \sim 10^{-7}$ mbar). Thus, the as-implanted and annealed samples were analyzed by scanning electron microscopy (SEM), transmission electron microscopy (TEM) and laser-pulsed atom probe tomography (LP-APT). SEM images were performed using a FEI Helios 600 Nanolab microscope in the secondary electron mode with an accelerating voltage of 5 kV. TEM images were obtained using a FEI Titan 80–300 Cs-corrected

* Corresponding author.
E-mail address: jacques.perrin-toinin@im2np.fr (J. Perrin Toinin).

http://dx.doi.org/10.1016/j.mssp.2015.07.082
1369-8001/

microscope operating at 200 kV under multibeam conditions, with the Ge substrate aligned along the $<110>$ crystallographic direction [7]. APT analyses were performed using a LEAP 3000X HR microscope in the pulsed laser mode. The analysis was carried out at 20 K, with a laser pulse frequency of 100 kHz, using a laser power of 0.07 nJ. TEM and APT samples were prepared using a dual-beam FEI Helios 600 Nanolab focuss ion beam (FIB) setup [8].

3. Results and discussion

Fig. 1 presents SEM images acquired on the surface of the as-implanted sample. Unusual implantation-mediated clusters can be observed (Fig. 1a) [9]. These clusters exhibit a surface density of $\sim 5.3 \times 10^7$ cm^{-2} with sizes in the micron-scale ($\sim$ 0.5–2 μm). One can also note that they show facets that could suggest a possible crystalline structure. These clusters were analyzed by APT. Fig. 2a presents an APT volume of $\sim 60 \times 60 \times 90$ nm^3 from the bulk of one of the clusters. The clusters consist of Ge and O atoms detected as single Ge atoms (red dots) or as Ge_nO_m molecules (various stoichiometries from Ge_2O to GeO_2… in blue dots) in the mass spectra. The atomic bulk composition of the clusters was found to be 50%, consistent with the composition of a GeO oxide (Fig. 2b). The sample surface not covered with clusters presents the usual implantation-mediated honeycomb structure (Fig. 1b) obtained in case of large dose and/or heavy ion implantations in Ge [10]. In our sample, the pore average diameter is about 60 nm (Fig. 1b) and their average depth is about 100 nm (Fig. 3). The Ge walls separating the empty honeycomb cells are $\sim$20 nm-thick at maximum (Fig. 1b). These dimensions lead approximately to a maximum Ge atomic density smaller than $\sim 1.9 \times 10^{22}$ cm^{-3} in the porous layer, which is about 2.3 times smaller than the regular Ge bulk density ($\sim$ 4.42×10^{22} cm^{-3}). Fig. 3 presents a cross-sectional view of these two types of implantation-mediated defects. Despite the observation of facets on the GeO clusters, TEM cross-sections show

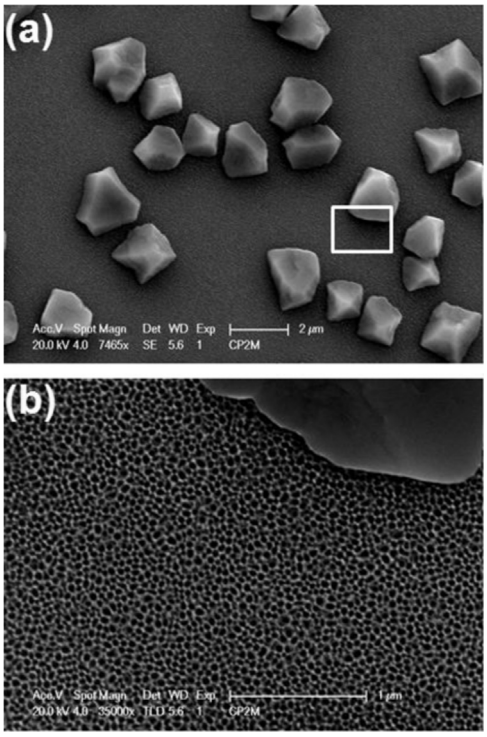

Fig. 1. SEM images of the as-implanted sample surface. The image (b) corresponds to the region delimited by a white solid line in the image (a) at higher magnification.

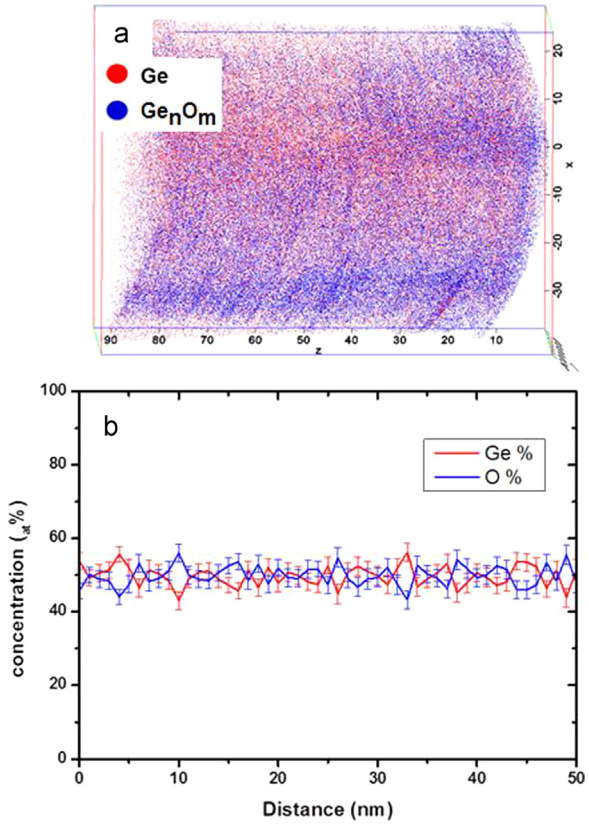

Fig. 2. APT measurements performed in the bulk of a surface implantation-mediated cluster: (a) $60 \times 60 \times 90$ nm^3 volume, red dots corresponds to single Ge atoms and blue dots corresponds to Ge_nO_m molecules; (b) one-dimensional atomic composition profile measured in the volume presented in (a). (For interpretation of the references to color in this figure legend, the reader is referred to the web version of this article.)

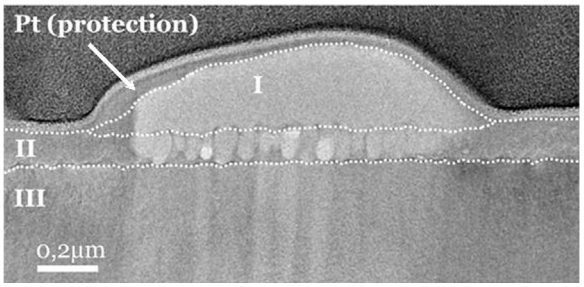

Fig. 3. TEM cross-sectional view of the as-implanted sample. The three regions noted I, II and III in the image correspond to a GeO cluster, the porous honeycomb structure, and the monocrystalline Ge substrate, respectively.

that the clusters are actually amorphous, suggesting that their facets are actually related to ion beam erosion instead of crystalline structure. The sample can be divided into three regions versus depth: (i) the first one corresponds to the amorphous GeO clusters ($\sim$ 300 nm-thick), (ii) the second one corresponds to the porous region forming a honeycomb structure from the sample surface up to a depth of $\sim$100 nm, and (iii) the third one corresponds to crystalline Ge (c-Ge). The TEM images evidenced the presence of the porous honeycomb structure underneath the GeO clusters, apparently filled with amorphous Ge oxide (Fig. 3). In addition, the TEM observations detected a high density of extended defects located below the porous layer, in the Ge crystal at a depth of 200 nm below the porous Ge/c-Ge interface.

After annealing at 650 °C for 1 h, the GeO clusters were still present on the sample surface (SEM observations not shown here).

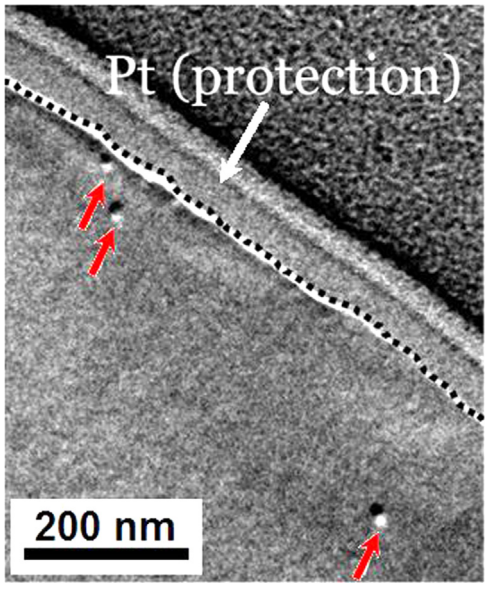

Fig. 4. TEM cross-sectional image of the Ge sample after Te implantation and annealing at 650 °C for 1 h. The dash line delimits the sample surface from the Pt protection layer deposited during FIB sample preparation. The red arrows highlight the presence of three dislocation loops. (For interpretation of the references to color in this figure legend, the reader is referred to the web version of this article.)

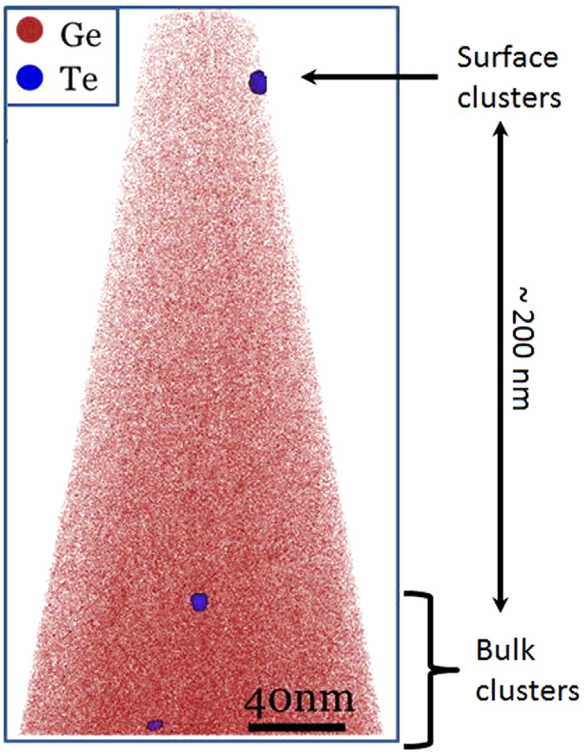

Fig. 5. APT volume ($150 \times 150 \times 300\ nm^3$) measured in the Te-implanted Ge sample after annealing at 650 °C for 1 h. Red dots correspond to single Ge atoms and the purple isoconcentration surfaces correspond to a Te atomic concentration of 1%. (For interpretation of the references to color in this figure legend, the reader is referred to the web version of this article.)

However, the porous honeycomb structure totally vanished, allowing for the epitaxial regrowth of crystalline Ge up to the sample surface. Fig. 4 shows a TEM cross-section image of the sample after annealing. The crystalline structure of the sample has recovered up to the sample surface (dashed line); however, dislocation loops are observed in the sample (red arrows). TEM observations showed that similar dislocation loops formed in the sample at two different depths during annealing. The dislocation loops exhibit diameters between 5 and 20 nm. The first dislocation distribution is located below the surface, in a ~70 nm-thick region, while the second dislocation distribution is located at a depth of ~200 nm below the surface. No Te–Ge cluster was detected by high resolution TEM. Contrasting with the results of TEM investigations, the results of the APT investigations did not detect dislocation loops, but show the presence of Te–Ge nano-clusters, once more highlighting the complementary aspect of TEM and APT investigation for nano-object detection [11,12]. The fact that APT analyses did not evidence the presence of dislocation loops can be related to the low dislocation loop density (APT field of view is significantly smaller than TEM field of view), as well as to the necessity of dislocations to be decorated with impurities [13–16] in order to be clearly distinguished (APT is more sensitive to chemistry than to microstructural variations). The fact that the nano-clusters were not detected by TEM [11] is probably due to the masking effect resulting from information overlapping through the TEM sample thickness, as well as due to the small size of the Te–Ge clusters. Indeed, the size of the Te–Ge clusters was found in the APT measurements to be comprised between 4 and 10 nm; however, due to local magnification effects resulting from a difference of evaporation field from the Ge matrix and the clusters [17–19], clusters could be actually smaller than observed in the APT volumes [13]. Fig. 5 presents an APT volume of $\sim 150 \times 150 \times 300\ nm^3$ measured in the Te-implanted sample after annealing. The red points correspond to Ge single atoms. Three Te–Ge clusters can be observed in this volume. In order to highlights these clusters, isoconcentration surfaces corresponding to 1% of Te (purple) are shown. No Te atom was detected between the Te–Ge clusters, meaning that solute Te atoms correspond to atomic concentrations smaller than the APT detection limit under the present analysis conditions ($\sim 5 \times 10^{19}\ cm^{-3}$ [12, 20]). The Te average concentration in the clusters was found to be $\sim 10 \pm 5$ at%. This concentration does not match the GeTe compound stoichiometry. However, due to the local magnification effects already mentioned, the compositions obtained by APT may contain a non-negligible error. In addition, it is important to note that due to the process used in the present work (implantation followed by annealing) the observed clusters are probably not the equilibrium nucleus of the GeTe phase, but unstable clusters that can form (and vanish) before phase nucleation [21]. Similar to dislocation loops, APT measurements shows that Te–Ge clusters are located at two different depths in the sample: (i) in a region close to the surface, and (ii) at a depth of ~200 nm below the surface. Combining TEM and APT results, two regions allowing defects such as dislocation loops and Te–Ge clusters to be formed during annealing can be observed in the samples, corresponding (i) to the region II in Fig. 3, related to the porous upper part of the as-implanted sample, and (ii) to the deep implanted-mediated defects in the region III in Fig. 3, at a depth of 200 nm in the as-implanted Ge substrate. These two locations correspond to regions experiencing important atomic redistribution during annealing (for example, the Ge lattice in the porous region is entirely recovered after annealing) that can act as point defect sources and sinks. Especially, dislocation loops are the signature of important Ge self-interstitial sources [22]. Te–Ge cluster formation at a depth of 200 nm proves that Te atoms were able to perform diffusion lengths long enough to reach the dislocation loops located at similar depth as clusters during annealing. Thus, one would expect dislocation loops to act as heterogeneous cluster nucleation centers, since heterogeneous nucleation is usually favored compared to bulk homogeneous nucleation. However, Te atoms decorating dislocation loops were not observed by APT and no cluster was found to be associated with a dislocation. After dislocation loop formation due to Ge self-

interstitials agglomeration, the Oswald ripening mechanism [16] should lead to a uniform distribution of dislocation loops, exhibiting the same size and a regular distance between them, due to Ge self-interstitial exchanges between dislocation loops. The fact that the detected dislocation loops exhibit a significant range of sizes (5–20 nm) means that the Oswald ripening phenomenon was not ended at the end of the thermal treatment. Thus, important self-interstitial flux can be expected during the annealing between the dislocations belonging to a same distribution (similar depth). Ge and Te atoms experiencing attractive interactions (formation of the TeGe compound), the formation of Te–Ge clusters between the dislocations loops can be explained by Te atom interactions with the Ge self-interstitial flux between dislocations. In this case, despite that Te–Ge cluster nucleation is not located on extended defects, cluster bulk nucleation does not corresponds to a regular homogeneous nucleation, but to a point defect-mediated bulk nucleation out of thermodynamic equilibrium (which can explain also why the Te–Ge clusters do not exhibit the TeGe phase stoichiometry). The reason why Te atoms do not segregate on dislocation loops triggering dislocation-mediated heterogeneous nucleation can be due to elastic interactions between substitutional Te atoms and the dislocation loops. Indeed, recent calculations [23] showed that substitutional sites surrounding dislocation loops in silicon experience strong compression states. For Te atoms corresponding to large and heavy atoms located on Ge substitutional sites, when in solution in Ge, the elastic field surrounding the dislocation loops may prevent Te accumulation in dislocation loop vicinity.

4. Conclusion

An 5×10^{15} cm^{-2} dose of Te atoms was implanted in Ge(001) in order to study the possible use of Te as *n*-type dopant in Ge. Te implantation leads to the formation of unusual amorphous GeO clusters on the Ge substrate surface, exhibiting sizes in the micrometer scale, as well as an important density of extended defects located 200 nm-deep in the Ge substrate bulk. In addition, Te implantation promotes the formation of a usual nano-porous region $\sim$70 nm-deep from the surface, already observed for other dopant implantation in Ge. Annealing at 650 °C for 1 h, leads to the formation of two distributions of dislocation loops and Te–Ge clusters located at two different depths in the sample: $\sim$35 and 200 nm. These depths appear to be related to the recrystallization of the porous region in the surface area and to the atomic redistribution surrounding the 200 nm-deep implantation-mediated extended defects. Te–Ge cluster formation between dislocation loops is assumed to be related to the interactions between diffusing Te atoms and Ge self-interstitial flux between dislocations involved in the dislocation loops' Oswald ripening process. The lack of Te segregation on Ge dislocation loops is expected to be due to the elastic field effect surrounding dislocation loops, preventing substitutional impurity accumulation. The quantity and the effects of Te implantation-mediated defects in Ge, lowering the concentration of solute Te atoms ($< 5 \times 10^{19}$ cm^{-3}) due to the formation of self-interstitial-mediated out-of-equilibrium Te–Ge clusters, prevent Te atoms to be used as Ge dopant via usual implantation methods.

Acknowledgments

This work was supported by the French National Agency for Research (ANR), France through the Program “Science de l’ingénierie” (Project DoGeTec, no. ANR-12-JS09-0015-1).

References

[1] S.M. Sze, Physics of Semiconductor Devices, Wiley-VCH, Berlin, 1981 2nd ed.
[2] C. Claeys, E. Simoen, Germanium-based Technologies: From Materials to Devices, Elsevier, Amsterdam, 2007.
[3] C. Claeys, E. Simoen, K. Opsomer, D.P. Brunco, M. Meuris, Mater. Sci. Eng. B 154–155 (5) (2008) 49.
[4] M. Meuris, A. Delabie, S. Van Elshocht, S. Kubicek, P. Verheyen, B. De Jaeger, J. Van Steenbergen, G. Winderickx, E. Van Moorhem, R.L. Puurunen, B. Brijs, M. Caymax, T. Conard, O. Richard, W. Vandervorst, C. Zhao, S. De Gendt, T. Schram, T. Chiarella, B. Onsia, I. Teerlinck, M. Houssa, P.W. Mertens, G. Raskin, P. Mijlemans, S. Biesemans, M.M. Heyns, Mater. Sci. Semicond. Process. 8 (1–3) (2005) 203.
[5] S. Gaudet, C. Detavernier, A.J. Kellock, P. Desjardins, C. Lavoie, J. Vac. Sci. Technol. A 24 (2006) 474.
[6] K. Romanjek, L. Hutin, C. Le Royer, A. Pouydebasque, M.-A. Jaud, C. Tabone, E. Augendre, L. Sanchez, J.-M. Hartmann, H. Grampeix, V. Mazzocchi, S. Soliveres, R. Truche, L. Clavelier, P. Scheiblin, X. Garros, G. Reimbold, M. Vinet, F. Boulanger, S. Deleonibus, Solid-State Electron. 53 (7) (2009) 723.
[7] M. Texier, J. Thibault-Pénisson, J. Micron 43 (2012) 516.
[8] A. Portavoce, K. Hoummada, A. Ronda, D. Mangelinck, I. Berbezier, J. Beilstein, Nanotechnology 5 (2014) 2374.
[9] J. Perrin Toinin, A. Portavoce, K. Hoummada, M. Texier, M. Bertoglio, S. Bernardini, L. Chow, J. Beilstein, Nanotechnology 6 (2015) 336.
[10] I.H. Wilson, J. Appl. Phys. 53 (1982) 1698.
[11] A. Portavoce, O. Abbes, A. Spiesser, C. Girardeaux, L. Michez, V. Le Thanh, Scr. Mater. 100 (2015) 70.
[12] A. De Luca, A. Portavoce, M. Texier, C. Grosjean, N. Burle, V. Oison, B. Pichaud, J. Appl. Phys. 115 (2014) 013501.
[13] K. Thompson, P.L. Flaitz, P. Ronsheim, D.J. Larson, T.F. Kelly, Science 317 (2007) 1370.
[14] S. Duguay, T. Philippe, F. Cristiano, D. Blavette, Appl. Phys. Lett. 97 (2010) 242104.
[15] K. Hoummada, D. Mangelinck, B. Gault, M. Cabié, Scr. Mater. 64 (2011) 378.
[16] K. Hoummada, G. Tellouche, I. Blum, A. Portavoce, M. Descoins, D. Mangelinck, Microelectron. Eng 107 (2013) 184.
[17] M.K. Miller, J. Phys. Colloq. 48 (1987) C6–565.
[18] F. Vurpillot, A. Bostel, D. Blavette, Appl. Phys. Lett. 76 (2000) 3127.
[19] G. Sha, A. Cerezo, Ultramicroscopy 102 (2005) 151.
[20] A. Portavoce, I. Blum, D. Mangelinck, K. Hoummada, L. Chow, V. Carrond, J. L. Làbàr, Scr. Mater. 64 (2011) 828.
[21] A. Pimpinelli, J. Villain, Physics of Crystal Growth, Cambridge University Press, Cambridge, 1998.
[22] A. Claverie, S. Koffel, N. Cherkashin, G. Benassayag, P. Scheiblin, Thin Solid Films 518 (9) (2010) 2307.
[23] A. Portavoce, G. Tréglia, Acta Mater. 65 (2014) 1.tp